# Analytic Force Field for Clusters and Nanoparticles of Aluminum and Its Hydride

Qingfan Zhang,[1,2] Enoch Tang,[1] Yongjie Xi,[1] Bo Han,[2] Nicole Legenski,[1,3] Guadalupe Chalas,[3] Frankie Chan,[3,4] Hansong Cheng,[1,2,*] and Robert C. Forrey[3,†]

[1]*Department of Chemistry, National University of Singapore, 3 Science Drive, Singapore 117543, Singapore*

[2]*Sustainable Energy Laboratory, China University of Geosciences, Wuhan, 430074, People's Republic of China*

[3]*Department of Physics, Pennsylvania State University, Berks Campus, Reading, Pennsylvania 19610-6009, USA*

[4]*Department of Mathematics, Purdue University, West Lafayette, Indiana 47906, USA*

(Received 11 March 2014; revised manuscript received 21 May 2014; published 18 June 2014)

An analytic potential energy function is developed for simulating clusters and nanoparticles of aluminum and its hydride. An embedded-atom method is used which modulates the background electron density as a function of the number of nearest-neighbor atoms. The method is parametrized and tested using an extensive training set computed from first-principle density-functional theory. The potential energy function is found to be reliable for clusters of arbitrary size, shape, and composition ratio. The force field obtained from the analytic potential energy function is computationally efficient and well suited for simulating large systems of aluminum and aluminum hydride particles. A proposed molecular dynamics simulation related to hydrogen-storage technologies for onboard automotive applications is briefly discussed.

DOI: 10.1103/PhysRevApplied.1.054004

## I. INTRODUCTION

There is growing interest in the use of hydrogen as an energy carrier, as it permits an efficient utilization of energy with zero emission of pollutants. Although much research is dedicated to finding novel methods of materials-based hydrogen storage through reversible physisorption or chemisorption processes, none of the materials that have been developed to date are able to meet the technical requirements for effective onboard hydrogen storage for vehicles [1]. Thus, most fuel cell vehicles powered by hydrogen today adopt the method of pressurized hydrogen storage using gas canisters which are generally composed of aluminum due to its light weight and high tensile strength. Light-duty vehicles normally contain 4 kg of hydrogen gas at 70 MPa (288.15 K) with a volumetric density of 40.2 g/l [2]. However, the embrittlement of materials caused by hydrogen diffusion may occur over time under these conditions, which can result in serious safety issues and become detrimental to the hydrogen economy. Because hydrogen is a colorless and odorless gas with a wide range of ignition temperatures, a high-pressure hydrogen gas leak can go undetected and cause a particularly exothermic explosion. Despite reinforcements of the aluminum canisters via an aluminum oxide coating, there may remain defective sites in the aluminum canisters that are prone to pitting attack by hydrogen. It is desirable, therefore, to develop robust and reliable means of safety evaluation for storage of high-pressure hydrogen within these canisters.

Molecular dynamics (MD) simulations can be used to investigate the interactions between hydrogen and aluminum surfaces and may provide an understanding of the mechanisms which lead to embrittlement. MD simulations generally rely on an atomic force field (FF) which is obtained as gradients of a potential energy function (PEF) that contain all relevant information of the atomic interactions for the system. First-principle electronic structure-based simulations are computationally challenging for systems which contain a large number of atoms, so it is often necessary to employ a model PEF which is analytic and transferable to clusters and nanoparticles of arbitrary sizes and shapes. The reliability of the model PEF depends on its ability to capture the essential bonding behavior and on the accuracy of the model parameters which are determined by theoretical or experimental data.

Embedded-atom (EA) methods based on density-functional theory (DFT) are commonly used to model atomic bonding in metallic systems. These methods are successfully applied to bulk metals [3–5] and in some cases are extended to metallic clusters and nanoparticles [6–9]. Although Al canister embrittlement for hydrogen storage is largely a defect problem in bulk Al, it is unlikely that a PEF fit to bulk Al will be accurate for performing the kind of safety studies envisioned here. Furthermore,

*Corresponding author.
chmch@nus.edu.sg
†Corresponding author.
rcf6@psu.edu

 

parametrization of a PEF using bulk data may lead to significant errors for the binding energies of small clusters and nanoparticles [10–13] which typically experience different local environments than their bulk counterparts. Since material formation processes may involve the coalescence of small clusters and nanostructures, it is generally desirable to develop analytic PEFs that are capable of describing clusters and nanoparticles of all sizes and shapes. Whereas aluminum clusters and nanoparticles have been investigated through first-principle calculations by various researchers [12–20], studies of binary compounds such as aluminum hydrides are less numerous. One important study [21] introduces a new valence-bond order (VBO) approach for modeling reactive potential energy surfaces. The VBO method is related to an EA method, and the initial application of the method to aluminum hydrides contains no explicit dependence on the bond angle or Coulombic terms in order to test and develop a simple functional form which would be well suited for large-scale simulations. Likewise, one of the motivations of the present study is to investigate the interactions between aluminum and hydrogen in the formation of aluminum hydrides so as to characterize and develop a general PEF form that properly accounts for both covalent and metallic bonding interactions. As in the previous study [21], the starting point for this investigation is to compute the energies for a large set of stable and metastable aluminum and aluminum hydride structures using first-principle DFT. These structures may then be used as a training set for determining the model parameters and testing the reliability of the FF for a variety of conditions.

## II. DFT CALCULATIONS

The calculations for the *ab initio* energies for many different cluster sizes of aluminum are performed using DFT under the generalized gradients approximation with the Perdew-Burke-Ernzerhof (PBE) exchange-correlation functional [22] as implemented in the DMOL3 package [23,24]. The electronic structure calculations are done using a double numerical atomic basis set augmented with a polarization function for valence electrons and an effective core potential to represent the core electrons. To test the accuracy of the chosen DFT method, the hybrid M06 functional [25] with the 6-311 + +G$(d, p)$ basis set as implemented in the GAUSSIAN09 package [26] is used to reoptimize the structures of several selected aluminum and aluminum hydride clusters. Comparison of the calculated average binding energies and the structural parameters obtained from the two DFT methods suggests that the difference is marginal (see the Supplemental Material [27]). The energy and gradient convergence tolerance is chosen to be $1 \times 10^{-7}$ Ha (hartree) and $2 \times 10^{-3}$ Ha/Å, respectively. The global orbital cutoff is set to 8.0 Å. A spin-polarized scheme is employed to deal with the electronically open-shell systems intrinsic to the Al atoms. All structures are fully optimized using the conjugate gradient algorithm without symmetry constraints.

An initial set of structures is generated by considering a variety of possible configurations with a small number of aluminum atoms in the cluster. The minimum energy structure for each subsequent cluster size is systematically determined by adding one atom to every possible site of the lowest-energy structures of the previous cluster size. The new atom is introduced only to regions that permitted the new atom to have three to five neighboring atoms, as well as a bond length of 1.5–3 Å away. This operation of sequentially adding one atom each time to generate clusters and then finding their *ab initio* energies is performed up to a cluster size of 30 aluminum atoms. Many of the new structures obtained as intermediate steps in the optimization procedure are introduced to the training set as well.

As the methodology involves the growth of aluminum clusters by stepwise addition to the most stable configuration of a smaller cluster, it is critical to determine the reliability of the method of cluster generation by comparing small clusters to the available literature. Ojwang *et al.* [19] found that $Al_4$ clusters typically form a rhombus conformation ($D_{2h}$), as compared to the pyramidal conformations ($C_{3v}$) proposed by Pettersson *et al.* [15]. The DFT calculations performed in this paper yield a small energy difference of −0.34 eV (5.1%) between the two configurations with the rhombus conformation being preferred and used for subsequent cluster generation. The optimized $Al_5$ cluster suggests that a two-dimensional structure continues to be the most stable, which is somewhat in line with the planar form found by Pettersson *et al.* [15], Yang *et al.* [17], and Ojwang *et al.* [19], whereas the three-dimensional structure proposed by Jug [16] suggests that a pyramidal form is the most stable. The energy difference between the two structures is small, implying that degeneracy might be observed between the two structures. The consensus of the above authors for $Al_6$ was an octahedral structure, although Upton [14] suggested a slightly distorted octahedral structure. The structure optimized via DFT calculations is a distorted octahedral as well. For $Al_7$, the most stable structure we obtain in the present work is a capped triagonal antiprism similar to Ojwang's structure. Böyükata and Güvenç [18] found the pentagonal bipyramid structure to be more stable by a small energy difference of 2.3 kcal/mol. The pentagonal bipyramid structure is not obtained by the sequential addition of atoms to a distorted $Al_6$ structure but is considered separately, and the difference in energy is found to be small between the two structures.

For $Al_{13}$, the structure we obtain from DFT optimization indicates that the lowest-energy configuration appears to adopt $I_h$ symmetry. This is consistent with Wang and Zhao [20] who used the same functional and correlation parametrization. However, Wang and Zhao also reported that a nonsymmetric $C_1$ configuration was found to be

energetically competitive with the $I_h$ structure, and the energy sequence depended on the choice of the exchange-correlation functionals. In general, the HF method or functionals with LYP correlation parametrization (BLYP, B3LYP, X3LYP) prefer the $C_1$ isomer, while the $I_h$ isomer is recognized as the lowest-energy structure by those functionals with Perdew's correlation parametrization, such as PW91, PBE, PBEO, B3PW91 [20]. These results imply that the theoretical lowest-energy structure of the atomic cluster is dependent on the choice of functional; however, the differences in the calculation of the binding energy for each cluster are small. PBE is chosen for this project as its ionization potentials, electron affinities, and bond lengths are of an accuracy similar to those obtained from empirical functionals, and it gives an accuracy comparable to the frequently used empirical B3LYP hybrid scheme [28]. All of the configurations calculated with the PBE exchange-correlation functional (both equilibrium and nonequilibrium structures) are included for the parametrization of the force field, which includes the $I_h$ and $C_1$ structures.

Larger cluster sizes are optimized and added to the training set such as hollow and solid spherical clusters in face-centered cubic (fcc) formation, bulk clusters with periodic boundary conditions, and randomly chosen intermediate-size clusters. The sequential addition of hydrogen atoms to small aluminum clusters is performed via a similar method. Hydrogen atoms are loaded onto minimum energy aluminum clusters until saturation, defined to be the point where hydrogen molecules form, is reached. The full aluminum hydride cluster is optimized for each new addition of hydrogen. Different loading sites are considered and have a strong influence on the relaxation of the underlying aluminum cage for small clusters. The DFT training set of aluminum and aluminum hydride structures is then used to determine the parameters of the model PEF as described below.

## III. MODEL

The general form of an embedded-atom PEF is given by

$$E = \sum_i \left[ \frac{1}{2} \sum_{j \neq i} V(r_{ij}) + F_i(\rho_i) \right], \tag{1}$$

where $V(r)$ is an effective two-body interaction, and $F_i$ is an energy functional that depends on the background electron density $\rho_i$ at site $i$. Generally, this energy functional represents the energy required to embed an atom into the background and, therefore, accounts for many-body effects. The pair potential and embedding functions are not unique, and it is sometimes convenient to define a reference structure for atom $i$ by renormalizing the background density with respect to the number of nearest neighbors [6]. In the present work, we normalize the background electron density with respect to a numerically determined function of the number of nearest neighbors. For aluminum hydride, we demonstrate the utility of this method by considering EA PEFs of the form

$$E = \sum_{i=1}^{N} d_i \left[ \frac{1}{2} \sum_{j \neq i} D_{IJ} \Phi_{IJ}^{(R)}(r_{ij}) - c_i \rho_i^{1/2} \right], \tag{2}$$

where $I$ is the type of atom at site $i$. We choose the convention $I = 1$ for aluminum atoms and $I = 2$ for hydrogen atoms. The square root of the densitylike quantity

$$\rho_i = \sum_{j \neq i} \Phi_{IJ}^{(A)}(r_{ij}) [\delta_{I1} \delta_{IJ} + \delta_{I2}] \tag{3}$$

provides the embedding function that accounts for the many-body effects. The $\delta_{I1}\delta_{IJ}$ term in Eq. (3) is used to model monatomic aluminum clusters, and the $\delta_{I2}$ term is used to correct the model when hydrogen is present. The attractive and repulsive pair potentials $\Phi_{IJ}^{(A)}$ and $\Phi_{IJ}^{(R)}$ are assumed to be universal for all clusters. Parametrization of an EA PEF using bulk data, however, may yield poor performance for small clusters [10–13]. The variation of metallic bonds for different cluster sizes and shapes is typically too large to be adequately described by a fixed set of pair parameters and constant coefficients $c_i$ and $d_i$. To overcome this difficulty, parameters that depend on the local environment are used in a Morse-type PEF [10] and in an EA-type PEF [11], and the agreement with *ab initio* DFT calculations is greatly improved. This additional flexibility, however, requires a large number of parameters and introduces small discontinuities in the force field for atomic configurations which are far from equilibrium. Here, we modify the approach taken in Ref. [11] and find good agreement with DFT results using a reduced set of parameters. The modified approach also provides continuity of the force field and its derivative for all possible configurations. In this method, the coefficients $c_i$ and $d_i$ are the only parameters that are allowed to depend on the number of nearest neighbors. The variation of these coefficients is equivalent to renormalizing the background density as described above. The force may then be calculated analytically from the EA PEF using

$$\begin{aligned} F_{x_i} &= -\frac{\partial E}{\partial x_i} \\ &= -\frac{1}{2} \sum_{j \neq i} \left[ (d_i + d_j) D_{IJ} \frac{\partial \Phi_{IJ}^{(R)}}{\partial r_{ij}} - c_i d_i \rho_i^{-1/2} \frac{\partial \rho_i}{\partial r_{ij}} \right. \\ &\quad \left. - c_j d_j \rho_j^{-1/2} \frac{\partial \rho_j}{\partial r_{ij}} \right] \frac{\partial r_{ij}}{\partial x_i} \\ &\quad + \sum_{j=1}^{N} \left[ \frac{\partial (c_j d_j)}{\partial x_i} \rho_j^{1/2} - \frac{1}{2} \sum_{k \neq j} D_{JK} \Phi_{JK}^{(R)} \frac{\partial d_j}{\partial x_i} \right]. \end{aligned} \tag{4}$$

The last term in Eq. (4) is zero for conventional EA methods which use constant coefficients. Because EA methods generally perform well for large clusters and bulk systems, this last term should tend to zero as the number of nearest neighbors increases to the bulk limit. However, when the number of nearest neighbors is small, this term may be used to improve the accuracy of the force field.

The computational effort required to calculate the force field may be reduced by eliminating large-distance contributions using the definitions

$$\Phi_{IJ}^{(R)}(r_{ij}) \equiv f_c(r_{ij}) V_{IJ}^{(R)}(r_{ij}), \tag{5}$$

$$\Phi_{IJ}^{(A)}(r_{ij}) \equiv f_c(r_{ij}) V_{IJ}^{(A)}(r_{ij}), \tag{6}$$

where $f_C$ is a smooth cutoff function. Following Ref. [6], we use

$$f_{a;b}(r) = \begin{cases} 1, & r \le a \\ \frac{1}{2}(1+x) - \frac{5}{8}x(x^2-1) & \\ \quad + \frac{3}{16}x(x^4-1), & a \le r \le b \\ 0, & r \ge b, \end{cases} \tag{7}$$

with

$$x = \frac{2r - a - b}{a - b}. \tag{8}$$

The function $f_{a;b}(r)$ has vanishing first and second derivatives at the connection points $r = a$ and $r = b$. For aluminum clusters, we find it convenient to use $f_c(r_{ij}) = f_{3;7}(r_{ij})$ for all pair interactions. This choice of cutoff function preserves the diatomic well and provides a smooth falloff which is built into the functional form of the pair potentials. The cutoff distance $b = 7$ is shown [12] to introduce negligible error for aluminum clusters. The analytic function $f_{a;b}(r)$ is also used to compute coordination numbers $M_i$ and $N_i$ for an atom $i$ from the definition

$$\sum_{j \ne i} f_{a;b}(r_{ij}) \equiv \begin{cases} M_i, & I = J \\ N_i, & I \ne J \end{cases}, \tag{9}$$

which allows the number of neighboring atoms to be counted with a weighting that depends on the distance. In Eq. (9), the choice $b = 7$ is used in order to be consistent with the cutoff function. However, the choice $a = 5$ is made so that rescaling the background electron density does not interfere with many-body effects which are already accounted for by the embedding function. Equation (7) is then further used to define the smooth step function

$$S_n(x) = 1 - f_{n;n+1}(x), \tag{10}$$

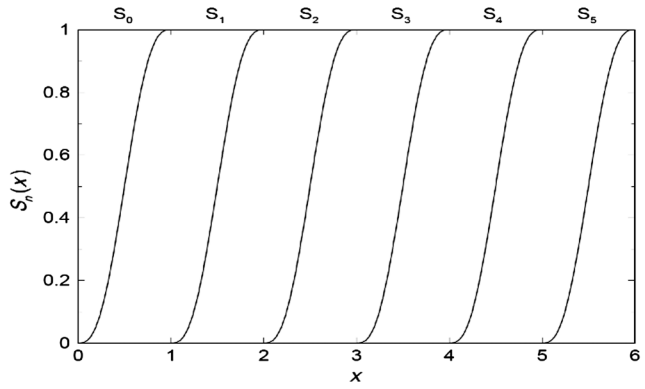


FIG. 1. Series of smooth step functions used to rescale the coefficient $c_i$ for atoms with fewer than six nearest neighbors.

which facilitates the variation of the coefficients in the EA PEF (2) when $x = M_i$ (see Fig. 1). For aluminum hydride clusters, we use

$$\begin{aligned} c_i = {} & [C_0 S_0(M_i) + \sum_{n=1}^{10} (C_n - C_{n-1}) S_n(M_i)] \delta_{I1} \\ & + [A_0 S_0(M_i) + B_0 S_0(N_i) + B_1 S_1(N_i) \\ & + B_2 S_0(M_i) S_0(N_i) + B_3 S_0(M_i) S_1(N_i) \\ & + B_4 S_1(M_i) S_0(N_i) + B_5 S_1(M_i) S_1(N_i) \\ & + B_6 S_0(M_i) S_2(N_i) + B_7 S_1(M_i) S_2(N_i) \\ & + B_8 S_2(M_i) S_2(N_i) + B_9 S_4(M_i) S_2(N_i) \\ & + B_{10} S_6(M_i) S_2(N_i)] \delta_{I2} \end{aligned} \tag{11}$$

and $d_i = D_0^{(I)}$. The series of smooth steps effectively interpolates $c_i$ from diatomic molecule parameters $A_0$, $B_0$, and $C_0$ to the polyatomic cluster parameters $B_n$ and $C_n$ for $n > 0$. In this work, the coefficient $d_i$ is held constant, which simplifies the force field and allows all small cluster renormalizations to be handled by the positive-definite coefficient $c_i$ of the attractive many-body contribution. For bare aluminum clusters, $c_i = C_{10}$ whenever atom $i$ has 11 or more neighbors within a radius of 5 Å. We find that this is sufficient to obtain a good description of all clusters sizes, including the fcc bulk limit.

For pure hydrogen, the H atoms prefer to form $H_2$ pairs, so the many-body effects are less important than in the case of pure aluminum. Therefore, the $c_i$ parameter in Eq. (11) may be assumed to be the constant value $A_0$ without modification when there is no aluminum present. The $B_n$ parameters allow the coefficient $c_i$ to depend on both the number and type of nearest neighbors. The number of step functions shown in Eq. (11) may be increased (or decreased) in order to provide more (or less) flexibility, as desired. In the present work, the many-body renormalizations are handled by the 20 parameters $B_n$ and $C_n$ for $n = 1$–10. The parameters $A_0$, $B_0$, and $C_0$ are fixed by the

pair potentials. Two examples of the attractive and repulsive pair potentials $V_{IJ}^{(A)}$ and $V_{IJ}^{(R)}$ are considered below.

### A. Example 1: QSC EA PEF

The quantum Sutton-Chen [29] (QSC) method uses pair potentials of the form

$$V_{IJ}^{(R)}(r_{ij}) = \left(\frac{\alpha_{IJ}}{r_{ij}}\right)^{p_{IJ}} \quad \text{and} \quad V_{IJ}^{(A)}(r_{ij}) = \left(\frac{\alpha_{IJ}}{r_{ij}}\right)^{q_{IJ}}.$$

The parameters $A_0, B_0, C_0, D_0$, and $D_{12}$ may be computed by setting the force equal to zero for the homonuclear and heteronuclear diatomic cases. The result is

$$A_0 = D_{22}\left(\frac{p_{22}}{q_{22}}\right)\left(\frac{\alpha_{22}}{r_{22}^*}\right)^{p_{22}-q_{22}/2}, \tag{12}$$

$$B_0 = \frac{D_0^{(1)} + D_0^{(2)}}{D_0^{(2)}} D_{12}\left(\frac{p_{12}}{q_{12}}\right)\left(\frac{\alpha_{12}}{r_{12}^*}\right)^{p_{12}-q_{12}/2}, \tag{13}$$

$$C_0 = D_{11}\left(\frac{p_{11}}{q_{11}}\right)\left(\frac{\alpha_{11}}{r_{11}^*}\right)^{p_{11}-q_{11}/2}, \tag{14}$$

$$D_0^{(I)} = \frac{E_{II}^*}{D_{II}}\left(\frac{\alpha_{II}}{r_{II}^*}\right)^{-p_{II}}\left(1 - \frac{2p_{II}}{q_{II}}\right)^{-1}, \tag{15}$$

$$D_{12} = \frac{2E_{12}^*}{D_0^{(1)} + D_0^{(2)}}\left(\frac{\alpha_{12}}{r_{12}^*}\right)^{-p_{12}}\left(1 - \frac{2p_{12}}{q_{12}}\right)^{-1}, \tag{16}$$

where $r_{IJ}^*$ is the equilibrium distance, and $E_{IJ}^*$ is the dissociation energy for the pair interaction between atoms of types $I$ and $J$. The pair parameters are symmetric with respect to $I$ and $J$, and $D_{II} \equiv 1$. Equations (12)–(16) show that the three diatomic molecules (two homonuclear and one heteronuclear) depend on the nine fitting parameters $\{\alpha_{IJ}, p_{IJ}, q_{IJ}\}$. These parameters are determined together with $B_n$ and $C_n$ for $n > 0$ by simultaneously fitting the energies for the whole set of cluster sizes and shapes as described in the next section.

### B. Example 2: Exponential EA PEF

An exponential EA method may be defined by the pair potentials

$$V_{IJ}^{(R)}(r_{ij}) = \exp\left(-\frac{r_{ij}}{\alpha_{IJ}}\right)^{p_{IJ}} \quad \text{and} \quad V_{IJ}^{(A)}(r_{ij}) = \exp\left(-\frac{r_{ij}}{\alpha_{IJ}}\right)^{q_{IJ}}. \tag{17}$$

As above, the force is set equal to zero for the homonuclear and heteronuclear diatomic cases. The result is the same upon making the substitution

$$\frac{\alpha_{IJ}}{r_{IJ}^*} \to \exp\left(-\frac{r_{IJ}^*}{\alpha_{IJ}}\right) \tag{18}$$

in Eqs. (12)–(16). Again, nine symmetric pair parameters $\{\alpha_{IJ}, p_{IJ}, q_{IJ}\}$ are determined together with $B_n$ and $C_n$ for $n > 0$ by simultaneously fitting the energies for the whole training set of cluster sizes and shapes.

## IV. RESULTS

For each aluminum cluster, the average binding energy per atom is calculated as

$$E_{\text{binding}} = [E(\text{Al}_n) - nE(\text{Al})]/n, \tag{19}$$

where $E(\text{Al}_n)$ is the energy of the entire cluster and $E(\text{Al})$ is the energy of a single aluminum atom. Figure 2 shows the result for the diatomic molecule. The present DFT results reproduce the well-known [30,31] double-well structure which arises from the crossing of the $^3\Pi_u$ and $^3\sum_g^-$ electronic states. The EA PEF depends on the choice of $r_{11}^*$ and $E_{11}^*$ as described above. Therefore, we try three alternative choices for these parameters: (i) fitting to the $^3\sum_g^-$ inner well, (ii) fitting to the $^3\Pi_u$ outer well, and (iii) fitting to a single smooth well which lies in between the two actual wells. This last alternative, which is consistent with the choice made by Jasper *et al.* [12], provides a broader well due to the repulsive and attractive sides of the well being taken from the two different electronic symmetries. In our attempts to find a PEF which describes

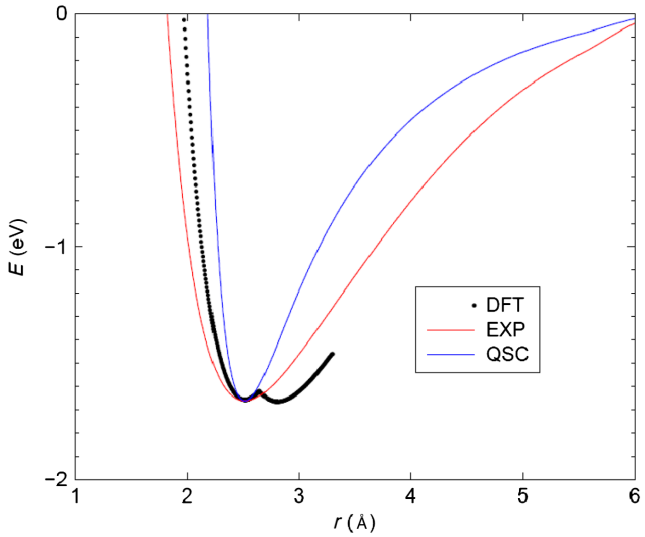


FIG. 2. Diatomic $Al_2$ potential. The points are DFT calculations which show the expected double-well structure [25,26]. The red curve corresponds to the exponential EA PEF, and the blue curve corresponds to the QSC EA PEF. Both models are constrained by the equilibrium parameters of the inner well. The nonequilibrium behavior is determined by the best fit to the whole training set of aluminum cluster sizes and shapes.

all aluminum cluster sizes and shapes, we find that alternative (i) works the best. Furthermore, although both of the EA PEFs considered in the present work are able to perfectly fit the repulsive and attractive sides of the inner well when only two atoms are included in the training set, our best results are obtained for all cluster sizes and shapes when the sides of the diatomic well are shifted (see figure). Interestingly, the QSC EA model gives a narrower well compared to the DFT data, whereas the exponential EA model gives a broader well. This is due to the smoother behavior of the exponential function in the transformation (18) as the distance approaches zero. The errors associated with the neglected double-well structure and the narrowing or broadening of the inner diatomic well are not expected to be important for molecular dynamics simulations. In both models, any diatomic molecules that break off from a large aluminum cluster will settle down to the equilibrium separation of the inner well, which yields an energy that is close to the accepted value.

To find the most stable structures for larger clusters, aluminum atoms are added sequentially to the stable clusters of the previous size starting with the diatomic molecule. As noted above, aluminum clusters are found to form three-dimensional structures with a size of six or greater. There is no noticeable pattern of cluster growth, and the aluminum structures generated for larger cluster sizes typically lack any high-order symmetry. The minimum energy structures that we find in the present work are shown in Fig. 3. These results are in contrast to the more symmetric structures found by Li *et al.* [32]. Whereas the sequential addition method is the primary method used for cluster generation in the present work, the methods used in Ref. [32] consist of the big bang (BB) searching algorithm [33] as well as the molecular dynamics simulation and quenching method (MDSQ). Both the BB and MDSQ methods [32] employ the NP-B [13] potential, which assumes that the electronic energy is separable and the average electronic excitation energy is independent of cluster size as well as isomer.

The set of minimum energy aluminum structures shown in Fig. 3 is augmented with a large number of nonequilibrium configurations of various sizes and shapes to form a training set for constraining the model FF. The monatomic aluminum parameters are obtained by computing the function

$$f(N) = \frac{\sum_m^{M_N} w_m |E_m^{\mathrm{DFT}} - E_m^{\mathrm{FF}}|}{N \sum_m^{M_N} w_m}, \tag{20}$$

where $M_N$ is the number of cluster configurations of size $N$, and $E_m^{\mathrm{DFT}}$ and $E_m^{\mathrm{FF}}$ are the respective DFT and model FF energies for the $m$th configuration. The weight function is chosen to be the absolute value of the DFT energy per atom. This weighting emphasizes the lowest-energy equilibrium structures without significantly neglecting the nonequilibrium structures and metastable isomers. Higher-energy structures are also fairly well described in most cases using

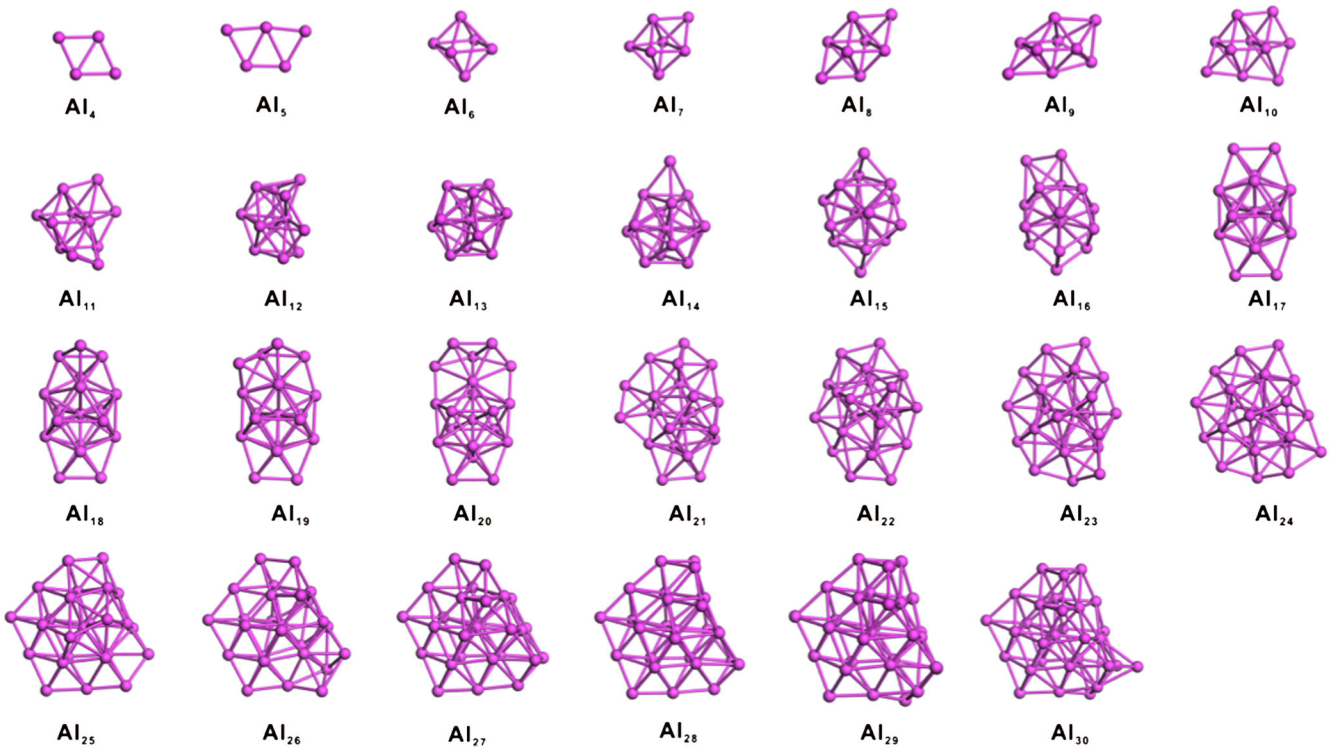


FIG. 3. Minimum energy structures for aluminum clusters computed by DFT.

TABLE I. Pair parameters for the EA PEFs.

| Type | | QSC | | | Exponential | | | Diatomic | |
|---|---|---|---|---|---|---|---|---|---|
| $I$ | $J$ | $\alpha_{IJ}$ | $p_{IJ}$ | $q_{IJ}$ | $\alpha_{IJ}$ | $p_{IJ}$ | $q_{IJ}$ | $r^*_{IJ}$ | $E^*_{IJ}$ |
| 1 | 1 | 2.829 46 | 13.429 59 | 6.635 43 | 2.559 34 | 7.090 26 | 3.217 35 | 2.513 | −1.662 |
| 2 | 2 | 1.842 57 | 2.389 50 | 3.477 97 | 1.175 46 | 3.910 62 | 5.952 33 | 0.750 | −4.547 |
| 1 | 2 | 2.391 65 | 6.926 77 | 4.703 47 | 3.619 80 | 11.173 93 | 10.536 84 | 1.685 | −3.098 |

this procedure. All cluster sizes are trained simultaneously by minimizing the function

$$g = \frac{\sum_N^{N_{\max}} N f(N)}{\sum_N^{N_{\max}} N}. \tag{21}$$

The size-dependent weighting in Eq. (21) helps to ensure an appropriate limit as cluster sizes approach the bulk. The minimization is performed by repeated use of a quasi-Newton algorithm in a general descent method with gradient values computed by finite differencing. Each application of the algorithm allows up to 200 iterations to obtain a local minimum for $g$. The parameters are defined so that a parameter $P$ is updated by computing $P_{\text{new}} = P_{\text{old}} + \exp(-|x|)$, where $x$ is the optimal value which yields the local minimum, and $P_{\text{old}}$ equals the previous best value minus a small offset. This procedure allows $P_{\text{old}} - \text{offset} \le P_{\text{new}} \le P_{\text{old}} + 1$, which enables deeper local minima to be searched for with each new application of the algorithm. There is no guarantee that this approach will locate a global minimum; however, it is generally reliable for finding a set of parameters which satisfy the criteria that $g \ll 1$ for a well-designed PEF.

Following Jasper *et al.* [12], the bulk cohesive energy $E_b$ is approximated for a given lattice constant $a$ by computing the function

$$E_b(a) = \frac{N_1^{1/3} Q_{N_1}(a) - N_2^{1/3} Q_{N_2}(a)}{N_1^{1/3} - N_2^{1/3}}, \tag{22}$$

where $Q_N(a)$ is the cohesive energy for $N$ atoms in a large cubic structure comprised of several fcc unit cells in each direction. The unsigned error in the bulk cohesive energy

$$\epsilon_b = \tfrac{1}{2}[|E_b(a_m) - E_b^e| + |E_b(a_e) - E_b^e|] \tag{23}$$

is added to Eq. (21) prior to performing the minimization. In Eq. (23), the label $e$ refers to the experimental value, and the label $m$ refers to the lattice constant, which gives the minimum bulk cohesive energy when computed using Eq. (22). To allow the calculation of $\epsilon_b$ to be performed quickly during the minimization, we follow the method of Ref. [12] and fit $E_b(a)$ to a quadratic form using three different values of $a$ ($0.9a_e$, $1.0\,a_e$, $1.1a_e$). The experimental values are 4.022 Å for the lattice constant and −3.43 eV/atom for the cohesive energy [12]. Our DFT calculations with periodic boundary conditions give a lattice constant of 4.0495 Å and a cohesive energy of −3.474 eV/atom, which are both in good agreement with the experimental numbers. For consistency of our training set, we replace the experimental numbers in Eq. (23) with our DFT values. This procedure results in a lattice constant of 3.9077 Å and cohesive energy of 3.473 94 eV/atom for the QSC PEF, and a lattice constant of 4.0447 Å and cohesive energy of 3.473 96 eV/atom for the exponential EA PEF.

After the PEF is trained to fit the DFT data, the PEF is used to compute energy minima using all structures in the DFT training set as starting points for the optimization. This is a critical step in establishing the reliability of the FF, as it is not uncommon to obtain a PEF which provides a good fit to a limited set of DFT data but produces energy minima that are well below expectations. Typically, this occurs when the DFT training set does not include enough nonequilibrium structures with compressed bonds. In such cases, the DFT training set is updated to include the minimum energy structures obtained by the PEF and a retraining is performed. The final set of parameters are given in Tables I and II for both the QSC EA PEF and exponential EA PEF considered in this work. Figure 4 compares the average error per atom for the two types of PEFs as a function of cluster size $N$. Both models perform well for small $N$ due to the rescaling of the attractive coefficient $c_i$ in Eq. (11). However, both models yield minimum energy structures for $N = 4$ and $N = 5$ that are three dimensional, whereas the DFT calculations yield

TABLE II. Parameters for rescaling the many-body coefficient $c_i$.

| | QSC | | Exponential | |
|---|---|---|---|---|
| $n$ | $B_n$ | $C_n$ | $B_n$ | $C_n$ |
| 1 | −0.253 39 | 8.036 34 | −0.015 30 | 0.012 09 |
| 2 | −1.446 51 | 8.542 92 | −0.384 34 | 0.012 63 |
| 3 | 0.260 37 | 9.354 15 | 0.016 13 | 0.013 71 |
| 4 | 0.128 56 | 9.442 04 | 0.007 33 | 0.013 29 |
| 5 | 0.124 26 | 9.722 82 | 0.001 43 | 0.013 96 |
| 6 | 0.012 74 | 9.707 57 | 0.002 46 | 0.013 81 |
| 7 | −0.193 90 | 9.772 44 | −0.011 17 | 0.013 90 |
| 8 | −0.048 00 | 10.293 87 | 0.000 77 | 0.014 35 |
| 9 | 0.118 40 | 10.293 71 | 0.005 60 | 0.014 35 |
| 10 | 0.207 32 | 10.374 58 | 0.001 93 | 0.014 35 |

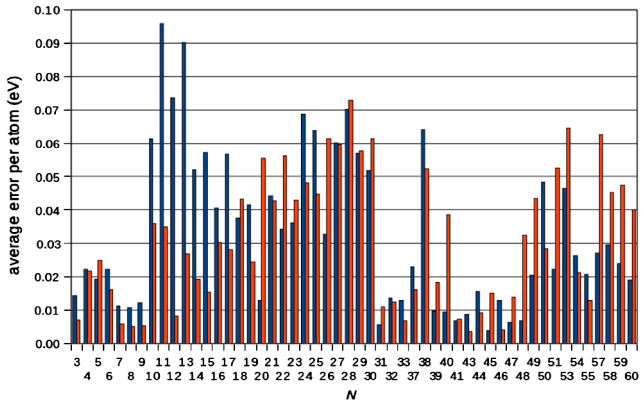


FIG. 4. Average error per atom as a function of Al cluster size. The left (blue) bars correspond to the QSC EA PEF, and the right (red) bars correspond to the exponential EA PEF. The error is computed by comparison with a DFT training set of bare aluminum clusters.

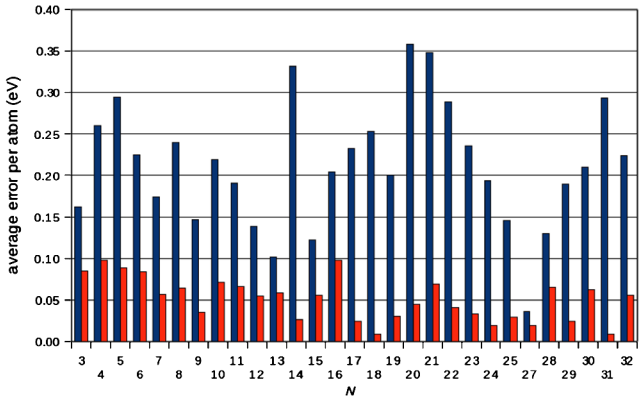


FIG. 5. Average error per atom as a function of $Al_mH_n$ cluster size $N = m + n$. The left (blue) bars correspond to the QSC EA PEF, and the right (red) bars correspond to the exponential EA PEF. The error is computed by comparison with a DFT training set of aluminum hydride clusters.

planar structures (see Fig. 3). In general, the optimized structures we obtain by the model PEFs tend to be more symmetric than those we obtain by the DFT calculations. Both models are able to keep the average error per atom below 0.10 eV for all cluster sizes and below 0.05 eV in most cases. The exponential EA PEF performs better than the QSC EA PEF, in agreement with previous observations [12]. Table II shows that $C_8 = C_9 = C_{10}$ for the exponential EA PEF, which indicates that $C_9$ and $C_{10}$ are not needed for this case. The mean unsigned error (MUE) for the QSC EA PEF is 0.041 eV/atom when the entire training set of clusters for $N \leq 60$ is used, but it increases to 0.068 eV/atom when the bulk error $\epsilon_b$ is included. For the exponential EA PEF, the bulk error is negligible, and the MUE is 0.035 eV/atom.

The parameters of the model aluminum hydride FF are determined by considering monatomic aluminum and hydrogen clusters in a first step. The parameters for the monatomic hydrogen FF are obtained using a training set consisting of different configurations of two and three hydrogen atoms whose energies were computed using DFT. Because H atoms prefer to form $H_2$ pairs, it is not necessary to include hydrogen clusters with more than three atoms in this training set. The second training step utilizes the monatomic parameters that are obtained in the first step. This step follows the minimization procedure described above, but now with a training set of binary clusters which consists of different configurations of $Al_mH_n$ with the combinations ($m = 1$, $n = 1$–4), ($m = 2$, $n = 1$–8), ($m = 3$, $n = 1$–8), ($m = 4$, $n = 1$–12), ($m = 6$, $n = 1$–18), and ($m = 8$, $n = 1$–24) whose energies were, again, computed using DFT. Figure 5 compares the average error per atom for the two types of PEFs as a function of cluster size $N = m + n$. The figure shows that the performance of the exponential EA PEF is now substantially better than the QSC EA PEF. Presumably, this is due to the smoother behavior of the exponential function compared to the inverse power law behavior which allows for broader wells in the aluminum hydride potential energy surface. The MUE for the exponential EA PEF is found to be 0.044 eV/atom when the full set of aluminum hydride clusters is used. The MUE for the QSC EA PEF is 0.22 eV/atom. This is clearly an unacceptably high error—the parameters for this model are given in the tables for comparison purposes only. It is recommended that only the exponential EA PEF be considered for use in molecular dynamics simulations that include hydrides. It is also noteworthy that the MUE for the VBO method [21] is found to be 0.1 eV/atom. Therefore, the exponential EA PEF appears to be the most reliable; however, the training set (and definition of MUE) are different in the two studies, so it is not possible to make this claim with certainty.

Figure 6 shows the diatomic potentials for AlH and $H_2$. The points are DFT calculations and the red curves correspond to the exponential EA PEF, which gives the best fit to the whole training set of cluster sizes and shapes. In both cases, the equilibrium position and well depth are fixed at the values obtained from the DFT calculations. The figure shows the model PEF for AlH is slightly narrower than the DFT results. The model PEF for $H_2$ shows a better fit to the DFT data in the well region but falls off more slowly with distance. The exact $H_2$ potential [34], which is shown in the figure for comparison, shows a deeper well than the results of the DFT calculation. For consistency, we use the DFT data in the training of the model FF.

Figure 7 shows the most stable structures for $AlH_3$ and $Al_2H_6$ that we obtain from DFT calculations and from the exponential EA PEF model. The planar $AlH_3$ molecule found in our DFT calculation agrees with the experimental structure found [35] at low temperature in a solid noble gas matrix. The same structure is obtained using the exponential EA PEF but with a slightly longer Al-H bond

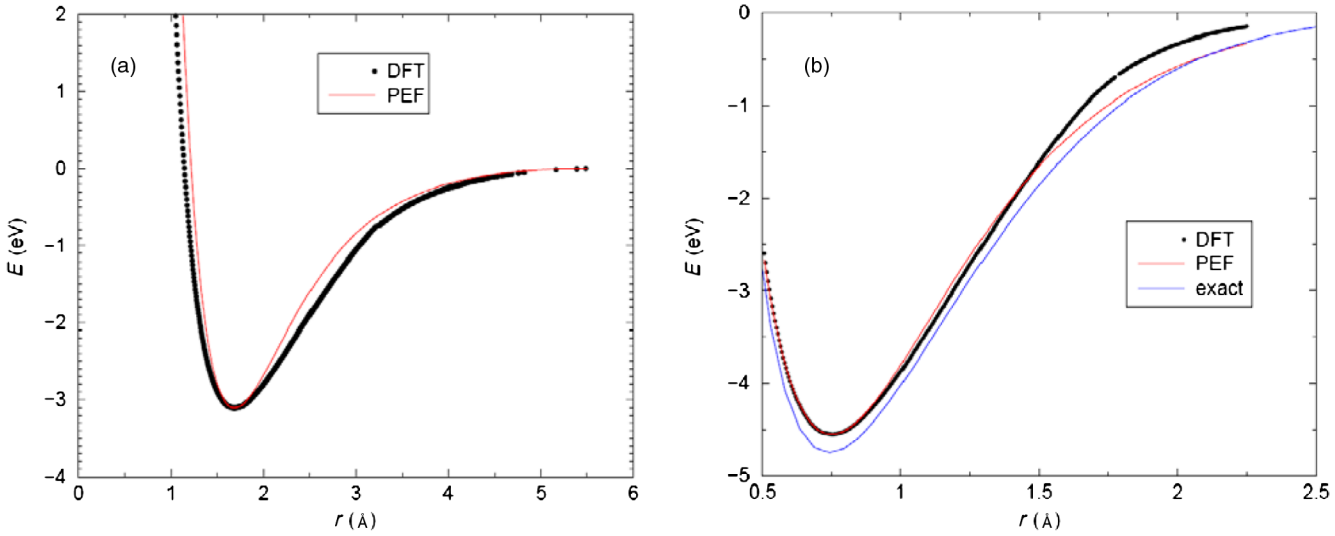


FIG. 6. Diatomic potentials for (a) AlH and (b) $H_2$. The points are DFT calculations, and the red curve corresponds to the exponential EA PEF which gives the best fit to the whole training set of cluster sizes and shapes. The exact potential for $H_2$ (blue curve) shows a slightly deeper well than the result of the DFT calculation.

length. For $Al_2H_6$, a similar increase of the Al-H bonds and also a decrease in the Al-Al bond are observed in the model PEF result. The structure of minimum energy cluster, however, remains the same.

In order to investigate the interaction of hydrogen and aluminum, small aluminum clusters are chosen. $Al_6$ and $Al_8$ are the smallest clusters that offer a high degree of symmetry, which permits any structural change to be easily observed and compared. Initial addition of $H_2$ to $Al_6$ occurs along the overlap of the HOMO of aluminum and the LUMO of the hydrogen molecule [see Fig. 8(a)], implying a charge transfer from $Al_6$. Various configurations are obtained for $Al_6H_2$, but the addition generally occurs along a corner of the $Al_6$ structure. The most stable configuration is shown in Fig. 8(b). Geometry optimization of oppositely placed hydrogen atoms for $Al_6H_2$ also results in a structure that has adjacent hydrogen. This suggests that the addition must involve the right symmetry of LUMO and HOMO and that the subsequent migration of the hydrogen atoms to the most stable configuration is favorable after the addition to the cage. The most stable configuration that we obtain by the model FF is shown in Fig. 8(c). The structure is, again, similar to the one we obtain by DFT but with slightly shifted bond lengths. The most stable structures from the first addition of $H_2$ to $Al_8$ found by DFT and the model FF are also illustrated in Figs. 8(b) and 8(c). The aluminum cage appears similar for the two calculations; however, the structure we find by the model FF shows H atoms bonded to three Al atoms, whereas the DFT result shows only two such bonds with a weak third bond between the H atoms

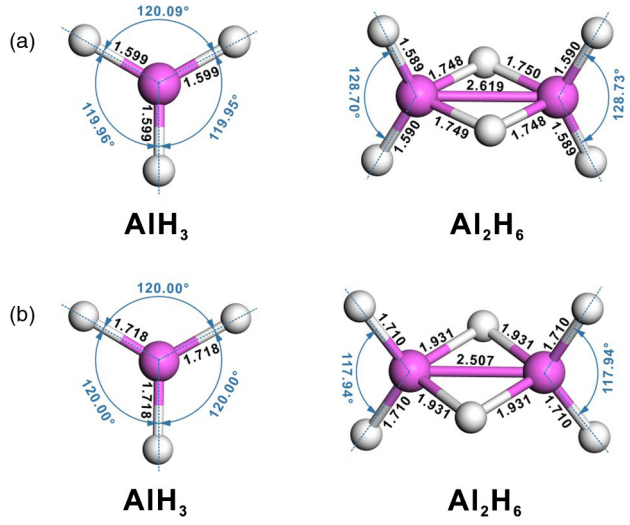


FIG. 7. Minimum energy structures for $AlH_3$ and $Al_2H_6$ clusters: (a) results from DFT calculation; (b) results from exponential EA PEF model.

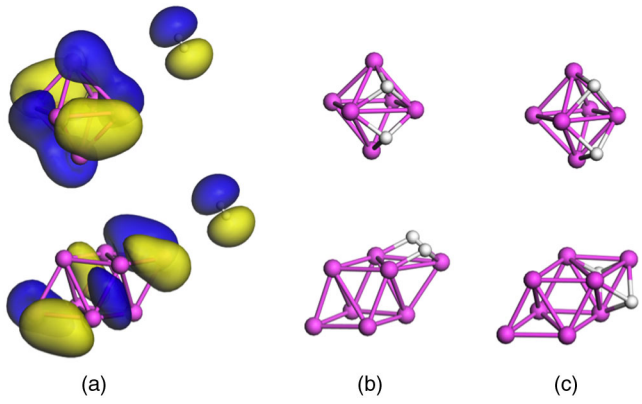


FIG. 8. (a) HOMO of $Al_6$ and $Al_8$ and LUMO of $H_2$; (b) most stable hydrides from first addition of $H_2$ computed by DFT; (c) most stable hydrides from first addition of $H_2$ computed by FF.

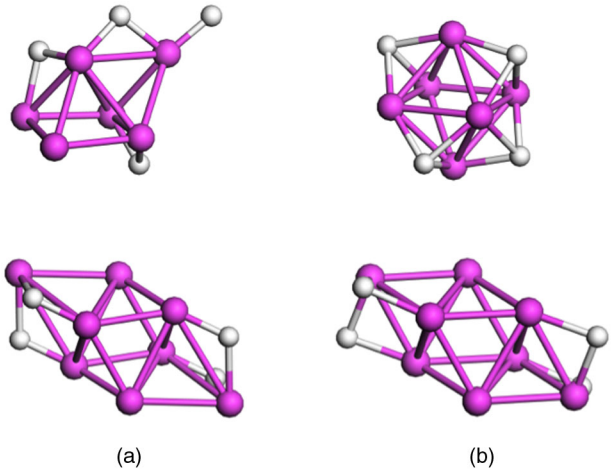


FIG. 9. (a) Most stable structures of $Al_6H_4$ and $Al_8H_4$ computed by DFT and (b) computed by FF. The FF result suggests the $Al_6$ cluster is able to maintain its original structure. DFT calculations reveal a metastable isomer for this configuration; however, a lower energy is obtained when the original $Al_6$ structure is distorted as shown. The original $Al_8$ structure is maintained in both DFT and FF calculations upon loading of four H atoms.

themselves. We do not consider this type of discrepancy to be a serious limitation of the model. There are many nearly degenerate aluminum hydride structures, and it is to be expected that there will be small discrepancies between the model and the exact results.

The addition of hydrogen to $Al_6H_2$ to form $Al_6H_4$ results in a distortion of the original structure when computed with DFT. This is shown in Fig. 9. The model FF does not predict the structure change obtained by DFT but instead simply attaches each of the four H atoms to three Al atoms of the original aluminum cage. The agreement is better for the addition of hydrogen to $Al_8H_2$ to form $Al_8H_4$, which is also shown in Fig. 9. In this case, the original aluminum cage is maintained, and the four H atoms are each attached to two Al atoms at the ends of the cluster. The subsequent addition of hydrogen to $Al_6H_4$ and $Al_8H_4$ results in further distortion of the octahedral structures. Beyond the initial addition of $H_2$ to form $Al_6H_2$ and $Al_8H_2$, it is difficult to discern any pattern of hydrogen addition, as similarities in terms of structural geometry can no longer be observed between the two clusters due to the different ways that the structures can be distorted. The most stable aluminum hydride structures are found, in general, to consist of a distortion of the initial aluminum cage with the attached hydrogen atoms spaced out as much as possible. As noted above, there are many nearly degenerate aluminum hydride structures. A sample of these isomers is included in the Supplemental Material [27].

The density of states of the aluminum hydride clusters is shown in Fig. 10 as a function of hydrogen loading. In each case, the metallic bonding in the bare clusters gradually changes to covalent bonding as the H loading increases. The maximum number of hydrogen atoms for both aluminum clusters is found to occur at a 1:3 ratio for Al:H. This saturation limit of the clusters is confirmed by molecular dynamics simulations at room temperature. Subsequent attempts to force additional hydrogen atoms onto the saturated clusters fail regardless of the site of addition. The exponential EA PEF is also tested for the hydride structures to see whether it can reproduce the correct H saturation limit for each aluminum cluster. In all cases, the model performs well and is able to find the correct saturation limit to within one or two H atoms. The model is also able to provide a good approximation to most of the structures obtained by the DFT calculations.

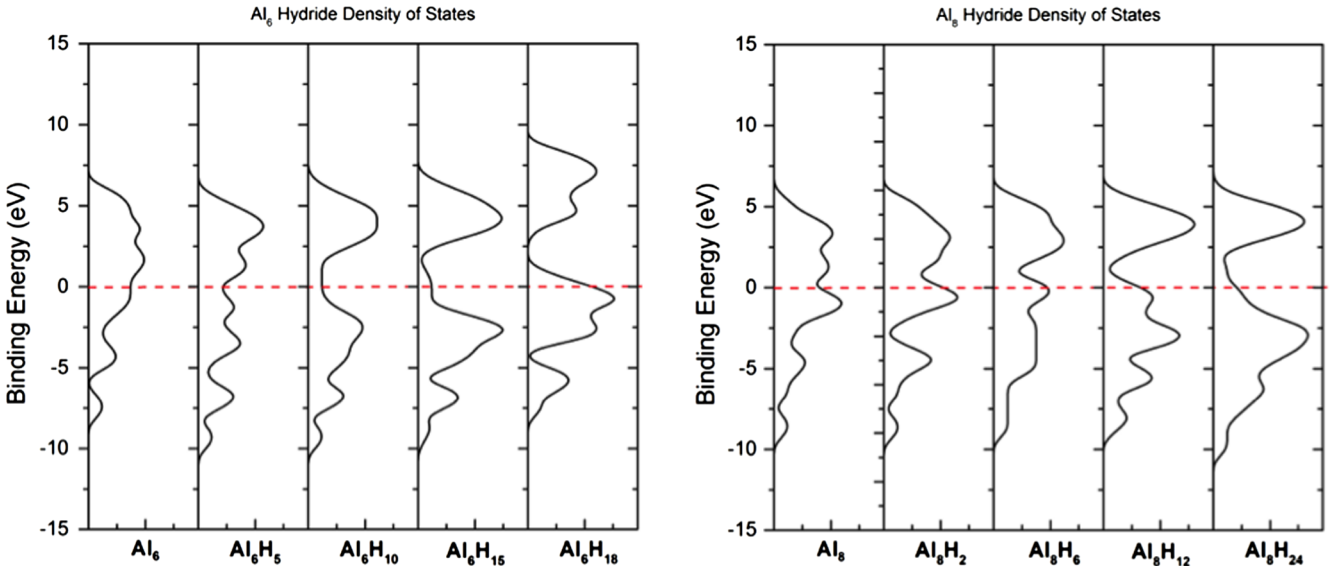


FIG. 10. Density of states for $Al_6$ and $Al_8$ clusters as a function of H loading.

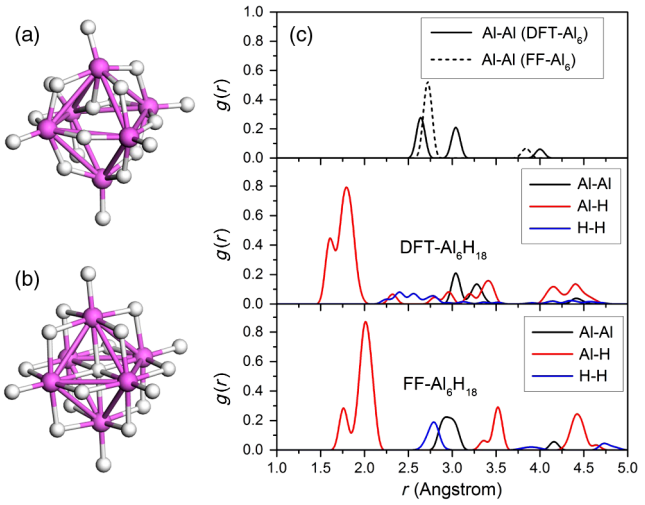


FIG. 11. (a) Structure of $Al_6H_{18}$ (fully saturated) obtained by DFT; (b) structure of $Al_6H_{18}$ obtained by FF; (c) radial distribution function of Al-Al, Al-H, and H-H for both $Al_6$ and $Al_6H_{18}$.

The optimized structure for $Al_6H_{18}$ is shown in Fig. 11(a). Interestingly, the aluminum cage is able to retain its original structure at saturation, whereas it is highly distorted when only four H atoms are attached to it [see Fig. 9(a)]. This is due to the loading method. When all four of the H atoms are loaded at the top sites, the $Al_6$ cluster is able to maintain its original structure. However, when the H atoms are loaded at the bridge or hollow sites, the aluminum bonds are distorted, and a structure transition produces a lower energy. While the model FF is not able to predict this structure change for the unsaturated $Al_6$ cluster, the FF is able to provide a good approximation of the optimized structure at saturation [see Fig. 11(b)].

In Fig. 11(c), the radial distribution function (RDF) is presented for the $Al_6$ and $Al_6H_{18}$ clusters obtained by DFT and FF. The RDF that we obtain by the model FF reveals a greater symmetry with respect to the H-H bonds and a small increase (approximately 0.2 Å) of the Al-H bonds, which is consistent with other cluster sizes (see Fig. 7). The RDFs that we compute by the two methods show comparable Al-Al bond lengths, which increase with the adsorption of hydrogen. This indicates weaker aluminum bonding in the fully saturated aluminum hydride compared to the bare cluster and suggests that hydrogen embrittlement occurs for small clusters. Furthermore, the DFT and model FF results both predict nearly degenerate isomers for the fully saturated cluster where one of the aluminum atoms has moved away from the core of the cluster as a result of the hydrogen addition, suggesting that aluminum atoms may become mobile upon hydride formation.

## V. CONCLUSIONS

An embedded-atom method is used to develop an analytic potential energy function for simulating clusters and nanoparticles of aluminum and its hydride. The method uses a single set of pair potentials for all cluster sizes but introduces a series of smooth step functions, which allow the background electron density to be scaled by the number of nearest-neighbor atoms. The parameters are determined by an extensive training set computed from first-principle DFT. The model FF that we obtain from the analytic PEF is computationally efficient and well suited for simulating large systems of aluminum and aluminum hydride particles. The force field can be used for large-scale molecular dynamics simulations to address whether the embrittlement of aluminum bonds as a result of the hydrogen addition will pose possible safety issues related to hydrogen-storage technologies for onboard automotive applications.

*Ab initio* molecular dynamics simulations based on DFT can only be used for small clusters and short time scales and, thus, are incapable of addressing the embrittlement phenomenon. Simulations that aim to study hydrogen embrittlement for large clusters and nanoparticles over long time scales will require a model FF which is physically realistic and computationally efficient. The model FF based on the exponential EA PEF that we develop in this work appears to be the best candidate for performing such large-scale simulations. The implementation of the model FF into the molecular dynamics codes is under way.

## ACKNOWLEDGMENTS

The work of N. L., G. C., F. C., and R. C. F. is supported by the National Science Foundation Grant No. PHY-1203228. N. L. also acknowledges support from Fulbright and NUS. We gratefully acknowledge support of the research by a NUS start-up grant, a Singapore National Research Foundation POC grant, and the Singapore-Peking-Oxford Research Enterprise, Grant No. COY-15-EWI-RCFSA/N197-1. Support from the National Natural Science Foundation of China (Grants No. 21203169 and No. 21233006) and the Fundamental Research Funds for the Central Universities, China University of Geosciences are also gratefully acknowledged.

[1] U.S. Department of Energy targets for onboard hydrogen-storage systems for light-duty vehicles, http://www1.eere.energy.gov/hydrogenandfuelcells/storage/pdfs/targets_onboard_hydro_storage.pdf.
[2] http://www.ika.rwth-aachen.de/r2h/index.php/Pressurized_Hydrogen_Refuelling.
[3] M. S. Daw and M. I. Baskes, Semiempirical, quantum mechanical calculation of hydrogen embrittlement in metals, Phys. Rev. Lett. **50**, 1285 (1983).
[4] M. S. Daw and M. I. Baskes, Embedded-atom method: Derivation and application to impurities, surfaces, and other defects in metals, Phys. Rev. B **29**, 6443 (1984).

[5] S. M. Foiles, M. I. Baskes, and M. S. Daw, Embedded-atom-method functions for the fcc metals Cu, Ag, Au, Ni, Pd, Pt, and their alloys, Phys. Rev. B **33**, 7983 (1986).
[6] M. I. Baskes, Modified embedded-atom potentials for cubic materials and impurities, Phys. Rev. B **46**, 2727 (1992).
[7] M. I. Baskes, J. S. Nelson, and A. F. Wright, Semiempirical modified embedded-atom potentials for silicon and germanium, Phys. Rev. B **40**, 6085 (1989).
[8] B. Lee and K. Cho, Extended embedded-atom method for platinum nanoparticles, Surf. Sci. **600**, 1982 (2006).
[9] B. Shan, L. Wang, S. Yang, J. Hyun, N. Kapur, Y. Zhao, J. B. Nicholas, and K. Cho, First-principles-based embedded atom method for PdAu nanoparticles, Phys. Rev. B **80**, 035404 (2009).
[10] C. Zhou, J. Wu, L. Chen, Y. Wang, H. Cheng, and R. C. Forrey, Force field for copper clusters and nanoparticles, J. Comput. Chem. **30**, 2255 (2009).
[11] N. Legenski, C. Zhou, Q. Zhang, B. Han, J. Wu, L. Chen, H. Cheng, and R. C. Forrey, Force fields for metallic clusters and nanoparticles, J. Comput. Chem. **32**, 1711 (2011).
[12] A. W. Jasper, P. Staszewski, G. Staszewska, N. E. Schultz, and D. G. Truhlar, Analytic potential energy functions for aluminum clusters, J. Phys. Chem. B **108**, 8996. (2004)
[13] A. W. Jasper, N. E. Schultz, and D. G. Truhlar, Analytic potential energy functions for simulating aluminum nanoparticles, J. Phys. Chem. B **109**, 3915 (2005).
[14] T. H. Upton, Structural, electronic, and chemisorption properties of small aluminum clusters, Phys. Rev. Lett. **56**, 2168 (1986).
[15] L. G. M. Pettersson, C. W. Bauschlicher, and T. Halicioglu, Small Al clusters. II. Structure and binding in Aln ($n = 2$–6, 13), J. Chem. Phys. **87**, 2205 (1987).
[16] K. Jug, Growth of small silicon and aluminum clusters, J. Mol. Struct. Theochem **202**, 277 (1989).
[17] S. H. Yang, D. A. Drabold, J. B. Adams, and A. Sachdev, First-principles local-orbital density-functional study of Al clusters, Phys. Rev. B **47**, 1567 (1993).
[18] M. Böyükata and Z. B. Güvenç, MD study of energetics, melting and isomerization of aluminum microclusters, Braz. J. Phys. **36**, 720 (2006).
[19] J. G. O. Ojwang, R. van Santen, G. J. Kramer, A. C. T. van Duin, and W. A. Goddard, Predictions of melting, crystallization, and local atomic arrangements of aluminum clusters using a reactive force field, J. Chem. Phys. **129**, 244506 (2008).
[20] L. Wang and J. Zhao, Which is the lowest-energy structure of Al13 clusters: Assessment of different exchange-correlation functionals in density functional theory, J. Comput. Theor. Nanosci. **6**, 449 (2009).
[21] M. Zhao, M. A. Iron, P. Staszewski, N. E. Schultz, R. Valero, and D. G. Truhlar, Valence-bond order (VBO): A new approach to modeling reactive potential energy surfaces for complex systems, materials, and nanoparticles, J. Chem. Theory Comput. **5**, 594 (2009).
[22] J. P. Perdew, K. Burke, and M. Ernzerhof, Generalized gradient approximation made simple, Phys. Rev. Lett. **77**, 3865 (1996).
[23] B. Delley, From molecules to solids with the DMol$^3$ approach, J. Chem. Phys. **113**, 7756 (2000).
[24] B. Delley, An all-electron numerical method for solving the local density functional for polyatomic molecules, J. Chem. Phys. **92**, 508 (1990).
[25] Y. Zhao and D. Truhlar, The M06 suite of density functionals for main group thermochemistry, thermochemical kinetics, noncovalent interactions, excited states, and transition elements: Two new functionals and systematic testing of four M06-class functionals and 12 other functionals, Theor. Chem. Acc. **120**, 215 (2008).
[26] M. J. Frisch *et al.*, GAUSSIAN09, Revision C01, Gaussian, Inc., 2009.
[27] See Supplemental Material at http://link.aps.org/supplemental/10.1103/PhysRevApplied.1.054004 for a comparison of the two DFT methods and a sample of aluminum hydride structures.
[28] M. Ernzerhof and G. E. Scuseria, Assessment of the Perdew-Burke-Ernzerhof exchange-correlation functional, J. Chem. Phys. **110**, 5029 (1999).
[29] A. P. Sutton and J. Chen, Long-range Finnis-Sinclair potentials, Philos. Mag. Lett. **61**, 139 (1990).
[30] S. R. Langhoff and C. W. Bauschlicher, Theoretical study of the spectroscopy of $Al_2$, J. Chem. Phys. **92**, 1879 (1990).
[31] Z. Fu, G. W. Lemire, G. A. Bishea, and M. D. Morse, Spectroscopy and electronic structure of jet-cooled $Al_2$ J. Chem. Phys. **93**, 8420 (1990).
[32] Z. H. Li, A. W. Jasper, and D. G. Truhlar, Structures, rugged energetic landscapes, and nanothermodynamics of $Al_n$ ($2 \leq n \leq 65$) particles, J. Am. Chem. Soc. **129**, 14899 (2007).
[33] K. A. Jackson, M. Horoi, I. Chaudhuri, T. Frauenheim, and A. A. Shvartsburg, Statistical evaluation of the big bang search algorithm, Comput. Mater. Sci. **35**, 232 (2006).
[34] A. Aguado, C. Suárez, and M. Paniagua, Accurate global fit of the H4 potential energy surface, J. Chem. Phys. **101**, 4004 (1994)
[35] F. A. Kurth, R. A. Eberlein, H. Schnockel, A. J. Downs, and C. R. Pulham, Molecular aluminium trihydride, $AlH_3$: Generation in a solid noble gas matrix and characterisation by its infrared spectrum and ab initio calculations, J. Chem. Soc. Chem. Commun. 1302 (1993).